Carbohydrate Polymers 370 (2025) 124371

Contents lists available at ScienceDirect

Carbohydrate Polymers

journal homepage: www.elsevier.com/locate/carbpol

Chain flexibility and branching effects on arabinogalactan conformation in solution

Hai Huang [a], Mengqi Wu [b], Rintaro Takahashi [a], Wenqing Zhang [b,*], Ken Terao [a,*]

[a] Department of Macromolecular Science, Graduate School of Science, The University of Osaka, 1-1 Machikaneyama-cho, Toyonaka, Osaka, 560-0043, Japan
[b] Shanghai Key Laboratory of Functional Materials Chemistry, School of Chemistry and Molecular Engineering, East China University of Science and Technology, Shanghai, 200237, PR China

ARTICLE INFO

Keywords:
Arabinogalactan
Small-angle X-ray scattering
Radius of gyration
Hydrodynamic radius
Form factor
Intrinsic viscosity

ABSTRACT

The structural and conformational characteristics of three arabinogalactans were investigated in aqueous and aprotic organic solutions using small-angle X-ray scattering (SAXS), dynamic light scattering, and viscosity measurements. This study aimed to clarify the dimensional and hydrodynamic properties related to the branching structure of a type II arabinogalactan extracted from jasmine tea leaves by comparing it with linear arabinogalactan (LG) and highly branched larch arabinogalactan (LAG60) samples. The obtained form factor $P(q)$ and the radius of gyration R_g for LG were analyzed in terms of the wormlike chain model with the Kuhn segment length of 2.80 nm, a measure of chain stiffness. This result indicates higher chain flexibility than that of polysaccharides whose backbone consists of 1,4-linked hexoses in a good solvent. The $P(q)$ data of the other two arabinogalactans, LAG60 and JSP-1a, which have short branches, were well described by the hyperbranched chain model. This model considers the fractal dimensions of partial chains in good solvent systems. The model uses a fixed number of branching points that exclude the contribution of single-sugar-residue branches. In addition, the hydrodynamic properties and the second virial coefficient were consistent with the $P(q)$ and R_g results.

1. Introduction

Arabinogalactan is a variety of polysaccharides commonly found in plants and some microorganisms (Saeidy et al., 2021). In general, it is present along the cell wall, associates with pectin or proteins (Silva et al., 2020), and plays an important role in cell growth, differentiation, signaling, etc. (Saeidy et al., 2021).

Many arabinogalactans from several plant materials have been studied over the years in terms of their primary structures (Huang et al., 2024; Ponder, 1998; Ponder & Richards, 1997), functionalities like immunomodulatory activity (Huang et al., 2023; Huang et al., 2024) and emulsification properties (Mora-Gutierrez et al., 2018), as well as the relationship between structure and function (Cheng et al., 2021; Villa-Rivera et al., 2021). While arabinogalactan proteins tend to form colloidal aggregates in aqueous media with distinctive shape features (Dror et al., 2006; Renard et al., 2014; Sanchez et al., 2008), little work has been done on the conformation of arabinogalactan (Mikhailenko et al., 2016; Quach et al., 2024) by means of small-angle X-ray scattering (SAXS). Furthermore, quantitative discussion for the dimensional properties of arabinogalactan with appropriate theories for branched polymers is still lacking.

Arabinogalactan chains are rich in galactose and arabinose residues, but exhibit high structural complexity due to multiple linkages on the β-D-galactopyranose backbone, high possibility of branching substitution, and diversity of residues on the branches. Based on the backbone linkages, arabinogalactans can be classified as type I (1,4-linked β-D-galactopyranose) (Hinz et al., 2005), type II (1,3-linked or 1,6-linked β-D-galactopyranose) (Huang et al., 2023; Ponder & Richards, 1997), or arabinogalactans whose backbone contains residues other than galactose residues (He et al., 2021; Zhang, Zhong, et al., 2019). In terms of branching patterns, most AGs exhibit a backbone substitution degree of approximately 38–100 % (Brecker et al., 2005; de Oliveira et al., 2013; Guo, Rao, & Wen, 2021; Liang et al., 2014; Xu et al., 2010), with values outside this range being relatively rare (Li et al., 2023). The branches are predominantly composed of galactose and arabinose, with occasional presence of rhamnose or uronic acids (Goellner et al., 2011; Peng et al., 2016). Regarding branch length, the branches typically consist of one to four sugar units, ranging from a single galactose or

* Corresponding authors.
E-mail addresses: zhwqing@ecust.edu.cn (W. Zhang), terao.ken.sci@osaka-u.ac.jp (K. Terao).

https://doi.org/10.1016/j.carbpol.2025.124371
Received 18 June 2025; Received in revised form 22 August 2025; Accepted 8 September 2025
Available online 9 September 2025

arabinose residue to a tetrasaccharide branch (He et al., 2018; Ponder & Richards, 1997), with occasional instances of extended and highly secondary-branched chains (Li et al., 2023). However, the substitution degree of single sugar residues on the backbone varies widely from 0 % (Li et al., 2023; Peng et al., 2016; Wang et al., 2015) to 100 % (Brecker et al., 2005; Suarez et al., 2005), whereas in recently reported type II AGs, the occurrence of di- or trisaccharide branches is notably high (He et al., 2021; He et al., 2018; Huang et al., 2024; Rakhmanberdyeva et al., 2021; Yao et al., 2018; Zhang, Zhong, et al., 2019). In our recent work, a 1,6-linked galactose-enriched type II arabinogalactan (JSP-1a) was isolated from jasmine tea processing waste (Huang et al., 2023), which exhibits potent immunomodulatory effects on certain macrophages. From its primary structure, the backbone shows a high degree of substitution by single sugar residues and possibly longer branches. To elucidate both the physicochemical properties and biological activities, conformational studies of JSP-1a, as well as those of other type II arabinogalactans, in aqueous media are indispensable.

We therefore investigated the dilute aqueous solution properties of JSP-1a by means of SAXS and viscometry. We chose different solvent systems because the solubility of JSP-1a in aqueous sodium chloride was not sufficiently high. For comparison, we also analyzed a commercially available type II arabinogalactan with predominantly 1,3-linked galactan chains, represented by the larch wood arabinogalactan (Ponder, 1998; Ponder & Richards, 1997), and a commercial polysaccharide enriched in 1,4-linked galactose-dominated chains. The latter corresponds to type I arabinogalactans. NMR measurements were also performed on the polysaccharide samples to confirm their primary structure.

2. Materials and methods

2.1. Materials

Three samples of plant polysaccharides were used in this structural conformation investigation. JSP-1a was isolated from jasmine tea processing waste as previously described (Huang et al., 2023). A larch arabinogalactan sample, LAG60, was prepared from commercially available larch arabinogalactan (TCI Chemicals) by fractional precipitation using water as solvent and ethanol as precipitant. A linear D-galactan sample, LG, was purchased from TCI chemicals, which had been developed for plant-based organic molecular catalysts (Takeuchi et al., 2018; Takeuchi et al., 2020). No further purification was performed on the sample.

2.2. Characterization of chemical composition and structure

The protein content of AG sample was measured by using the Bradford method (Bradford, 1976) with a calibration curve whose linear range is 1.57–25 μg/mL, while the ash content was estimated from the inorganic residue remaining after combustion in the CHN analyzer (YANACO, MT-6). The moisture levels were measured according to AOAC 930.15 that calculated the weight difference of samples before and after drying in an oven (135 °C, 2 h).

The monosaccharide composition of the three polysaccharides was analyzed by the PMP derivatization HPLC method with slight modifications (Huang et al., 2023). Briefly, after hydrolysis with 2 M aqueous TFA and PMP derivatization, the analytes were analyzed on an HPLC system equipped with a reversed-phase C_{18} column (GL Science Inert-Sustain C18, 4.6 × 150 mm, 3 μm) and eluted with a mobile phase of 19 % ACN/81 % aqueous 20 mM ammonium acetate at a flow rate of 1.0 mL/min.

The ^{1}H NMR and ^{13}C NMR spectra were recorded for LG and LAG60 in D_2O, using a 400 MHz NMR spectrometer (JEOL ECS400) to analyze their glycosidic linkages. The number of scans for ^{1}H NMR and ^{13}C NMR was set to 32 and 14,000, respectively.

2.3. Light scattering measurements

The weight-average (M_w), number-average (M_n) molar masses, and molar mass distribution ($Đ$) were determined using a size-exclusion chromatography (SEC) system (Shodex GPC-101) equipped with a refractive index detector (Shodex, Japan) and a multi-angle light scattering detector (DAWN HELEOS II, Wyatt Technology Co., USA), where the wavelength λ_0 of the incident light in a vacuum was 658 nm. A 100 μL of analyte was injected into a Shodex SB 804 HQ column and eluted with 0.1 M aqueous NaCl at a flow rate of 1.0 mL/min at 40 °C.

Static light scattering (SLS) and dynamic light scattering (DLS) measurements were performed simultaneously by using ALV/SLS/DLS-5000 light scattering photometer equipped with a Nd-YAG laser with $\lambda_0 = 532$ nm. Each sample solution was filtrated by a 0.20 μm cellulose acetate syringe filter, injected into 8 mm ϕ cylindrical cells and immersed in a xylene bath maintained at 25.0 °C. Toluene served as a reference standard to convert the measured excess scattering intensity at a fixed angle to the Rayleigh ratio.

The refractive index increment ($\partial n/\partial c$) of the sample at $\lambda_0 = 658$ nm and $\lambda_0 = 532$ nm was estimated in the same solvent at 25.0 °C using a Schulz-Cantow type differential refractometer over a polymer mass concentration c range of 0–10 mg/mL.

2.4. Viscosity measurements

The relative viscosity η_r and specific viscosity η_{sp} of the three polysaccharide samples in 0.1 M aqueous NaCl were measured at 25.0 °C using a conventional Ubbelohde viscometer, and calculated using the following equations. The Huggins and Mead–Fuoss plots were combined to analyze the experimental data to determine the intrinsic viscosity [η] and the Huggins coefficient k'.

2.5. Small-angle X-ray scattering (SAXS) measurements

SAXS measurements were carried out at the BL40B2 beamline in SPring-8 using a 2.0 ϕ mm quartz capillary cell fixed in an aluminum block. The solvent, a polyethylene oxide (PEO) standard (SE-5, Tosoh, Japan), and sample solutions were measured in the same capillary at 25.0 °C for 180 s. The λ_0 value for the incident X-ray and the sample-to-detector distance (camera length) were set to 0.1 nm and 4.2 m, respectively. SAXS profiles were recorded using a Dectris PILATUS3 2 M two-dimensional pixel detector and processed to the scattering intensity as a function of the magnitude q of the scattering vector, using the SAngler circular averaging software (Shimizu et al., 2016). Silver behenate was used to calibrate q for each pixel on the detector. The intensity of the incident X-ray was monitored both upstream and downstream of the solution cell to compensate for intensity fluctuations and X-ray transmission. This allowed for the evaluation of the scattering intensity $I(q)$ as a function of the magnitude q of the scattering vector. The excess scattering intensity $\Delta I(q)$ was calculated as the difference in $I(q)$ between the sample solution and the solvent.

The polysaccharide samples for SAXS measurements were dissolved in two aqueous media: 0.1 M aqueous NaCl and Hank's balanced salt solution without calcium and magnesium [HBSS(−)]. Dimethylacetamide (DMAc)/0.1 M LiCl was also attempted to dissolve the polysaccharide samples, but JSP-1a and LG were not analyzed due to significant aggregation in this media. Each sample solution was prepared at four different concentrations, all of which were well below the calculated overlap concentration c^* of 168, 756, and 113 mg/mL for JSP-1a, LAG60, and LG, respectively, and thus corresponded to the dilute regime. The ratio of excess scattering intensity to concentration $\Delta I(q)/c$ for each sample was independent of concentration except in the lowest q region (Fig. S1), suggesting sufficient repeatability.

The ratio of the reduced scattering intensity R_q to the X-ray optical constant K for 0.1 M aqueous NaCl and DMAc/0.1 M LiCl media was estimated from the following equation (Tomofuji et al., 2022) based on

the theory for SAXS (Glatter & Kratky, 1982).

$$\frac{R_q}{K} = M_{w,PEO}\left(\frac{\Delta z_{PEO}}{\Delta z}\right)^2 \left[\frac{c_{PEO}}{\Delta I_{PEO}(q)}\right]_{c\to 0, q\to 0} \Delta I\,(q) \quad (1)$$

Here, Δz is the difference between the number of moles of electrons per unit mass of the solute (z), and the subscript PEO indicates the value for the standard PEO solution.

Using the Berry plot, $(Kc/R_q)^{1/2}$ data are plotted against q^2 or c, M_w, the radius of gyration R_g and the second virial coefficient A_2 can be estimated by Eqs. (2) and (3), respectively.

$$\left(\frac{Kc}{R_q}\right)^{1/2}_{c=0} = \frac{1}{M_w^{1/2}}\left(1 + \frac{1}{6}R_g{}^2q^2 + O(q^4)\right) \quad (2)$$

$$\left(\frac{Kc}{R_0}\right)^{1/2} = \frac{1}{M_w^{1/2}}\left(1 + A_2M_wc + O(c^2)\right) \quad (3)$$

Since Δz is hard to estimate for HBSS(−) media because of the difficulty in calculating the electron density of glucose in HBSS(−) media, Kc/R_q was calculated using the M_w value determined by SEC-MALS.

3. Results and discussion

3.1. Chemical structure of polysaccharide samples

As shown in Table S1, the protein contents of LG, LAG60, and JSP-1a were ≤0.69 %, while the moisture levels were all below 1.55 %. Ash contents were 3.47 %, 0.70 %, and 2.65 %, respectively, which are within the range reported for isolated plant polysaccharides (Loosveld et al., 1997). These results indicate negligible protein, mineral, and moisture contents, suggesting that the three AGs are mainly composed of carbohydrate components. The monosaccharide composition profiles are shown in Fig. S2. Galacturonic acid and glucuronic acid were not detected in any of the three AGs, indicating that these AGs lack uronic acid residues and thus have negligible polyelectrolyte character. The monosaccharide compositions were further summarized in Table 1, where LG and LAG60 are mainly composed of galactose with low percentage of arabinose, whereas JSP-1a had higher percentage of arabinose that reached 33.9 %. The major linkages of LG were further investigated by ^{1}H and ^{13}C NMR. According to the patent (Wada et al., 2023), each LG molecule has 2–3 arabinose residues on its main linear galactan chain. The most prominent resonance signals in Fig. S3(A) appear at δ_H 4.20/δ_C 77.8, which are attributed to the fourth position of the 1,4-linked β-galactopyranose (1,4-β-Gal*p*) residue (Hinz et al., 2005; Wefers & Bunzel, 2016; Zhang, Chen, & Ding, 2019), indicating that 1,4-β-Gal*p* residues are prevalent in LG. Although the linkage of arabinose residues could not be further confirmed because of the weak signal around δ_H 4.95/δ_C 105, the arabinose content was relatively low. Thus, the primary structure of LG could be assumed to be an unbranched linear chain, as illustrated in Fig. S4(A).

The primary structure of larch arabinogalactan was well elucidated by Ponder et al. through selective hydrolysis of the backbone of the 1,3-linked β-galactan (Ponder & Richards, 1997) and methylation analysis of the resulting product (Ponder, 1998). The following structure was obtained as shown in Fig. S4(B). In this study, ^{1}H and ^{13}C NMR were also conducted on LAG60, and the results (Fig. S5) are almost identical to those reported by Ponder et al. (Ponder & Richards, 1997). Thus, this detailed primary structure can be used as a cornerstone for the subsequent SAXS analysis.

As for JSP-1a, its primary structure was investigated and compared with the data from previous research (Huang et al., 2023). Several key linkage points were identified based on coupled signals observed in the 2D NMR spectra, including the linkage of a terminal arabinose to the third position of 1,3,6-linked galactose on the backbone, terminal arabinose to 1,5-linked arabinose, and 1,3-linked galactose to 1,4-linked mannose. This analysis clarified the backbone structure but left some ambiguity regarding the branching linkages as shown in Fig. S4(C).

Table 1
Monosaccharide composition and molar mass (SEC-MALS) in 0.1 M aqueous NaCl.

Sample	LG	LAG60	JSP-1a
Galactose/%	96.1	85.7	59.6
Arabinose/%	3.9	14.3	33.9
$\partial n/\partial c$/mL g^{-1}	0.145	0.142	0.146
M_n/kg mol^{-1}	8.8	64.9	78.3
M_w/kg mol^{-1}	10.1	66.8	94.8
$Đ$	1.15	1.03	1.21

3.2. Dimensional properties in diluted solution

The average molar masses, M_w, M_n, and molar mass distribution ($Đ$) were determined by SEC-MALS in 0.1 M aqueous NaCl and are summarized in Table 1. As shown in Fig. 1, each sample exhibits a single and symmetrical chromatographic peak in the RI chromatogram. The measured values of M_w and M_n were all below 100 kg mol^{-1}, and $Đ$ values were less than 1.2, indicating that the resolution of the analytical column and separation methods were sufficient for three polysaccharides. However, an additional peak was observed in the light scattering signal around the retention volume $V_e = 6$ mL at the scattering angle of 90°, while no corresponding peak appeared in the RI channel. This indicates that a small amount of aggregates with extremely high M_w, possibly formed naturally in aqueous solution, produced a particularly strong light scattering intensity (Qin et al., 2013). These aggregates were also found in the slow component of the DLS data (Fig. S6) and in the upturn of the SAXS profiles (Fig. S1), similar to our recent study for a water-soluble polysaccharide derivative (Nakata et al., 2024). It should be noted that the MALS data for three AGs and the SLS data corresponding to the fast component ($R_{theta,fast}$) of LAG60 identified by DLS, showed minimal angular dependence, although the associated errors were too large to be tolerated (Fig. S7). Consequently, the gyration radius of these polysaccharides could not be obtained by light scattering techniques. The scattering intensity of the fast component was calculated from the scattering intensity and the area ratio of the peaks in Fig. S6 with the method reported elsewhere (Jinbo et al., 2003).

Although some aggregates were observed in 0.1 M aqueous NaCl solution, the M_w from SAXS and the radii of gyration (R_g) could still be determined from the linear low-q region of the extrapolated SAXS data, as indicated by the red dashed lines in the Berry plot (Fig. 2). The M_w values from SAXS are substantially consistent with those determined by SEC-MALS, considering the potential influence of aggregation and/or the error in the determination of $\partial n/\partial c$ and Δz.

Furthermore, the second virial coefficients (A_2) were estimated from the same scattering vector range (Fig. 2). Positive A_2 values for all polysaccharide samples in the corresponding solvent systems indicated that they are good solvent systems. The resulting data are summarized in Table 2. Additionally, LAG60 and JSP-1a showed similar R_g/R_H in different media, revealing similar conformational properties in the different media.

Moreover, the double logarithmic plot of R_g versus M_w is a useful tool for comparing different polysaccharides. As displayed in Fig. 3, all R_g data, including both the present measurements and literature values, were obtained under good solvent conditions at temperature between 20 °C and 25 °C. The R_g of LG closely matches that of pullulan in aqueous media (Kato et al., 1984; Watanabe & Inoko, 2011), pullulan in 0.25 M LiCl/DMSO (Tao et al., 2009), amylose in DMSO (Nakanishi et al., 1993), and curdlan in 0.25 M LiCl/DMSO (Tao et al., 2009), all of which are typical flexible linear polysaccharides with the same M_w. This suggests that LG is a linear polysaccharide, as deduced from the NMR analysis described above. The R_g data of LAG60 in three solvents are slightly higher than those of glycogen, a highly branched

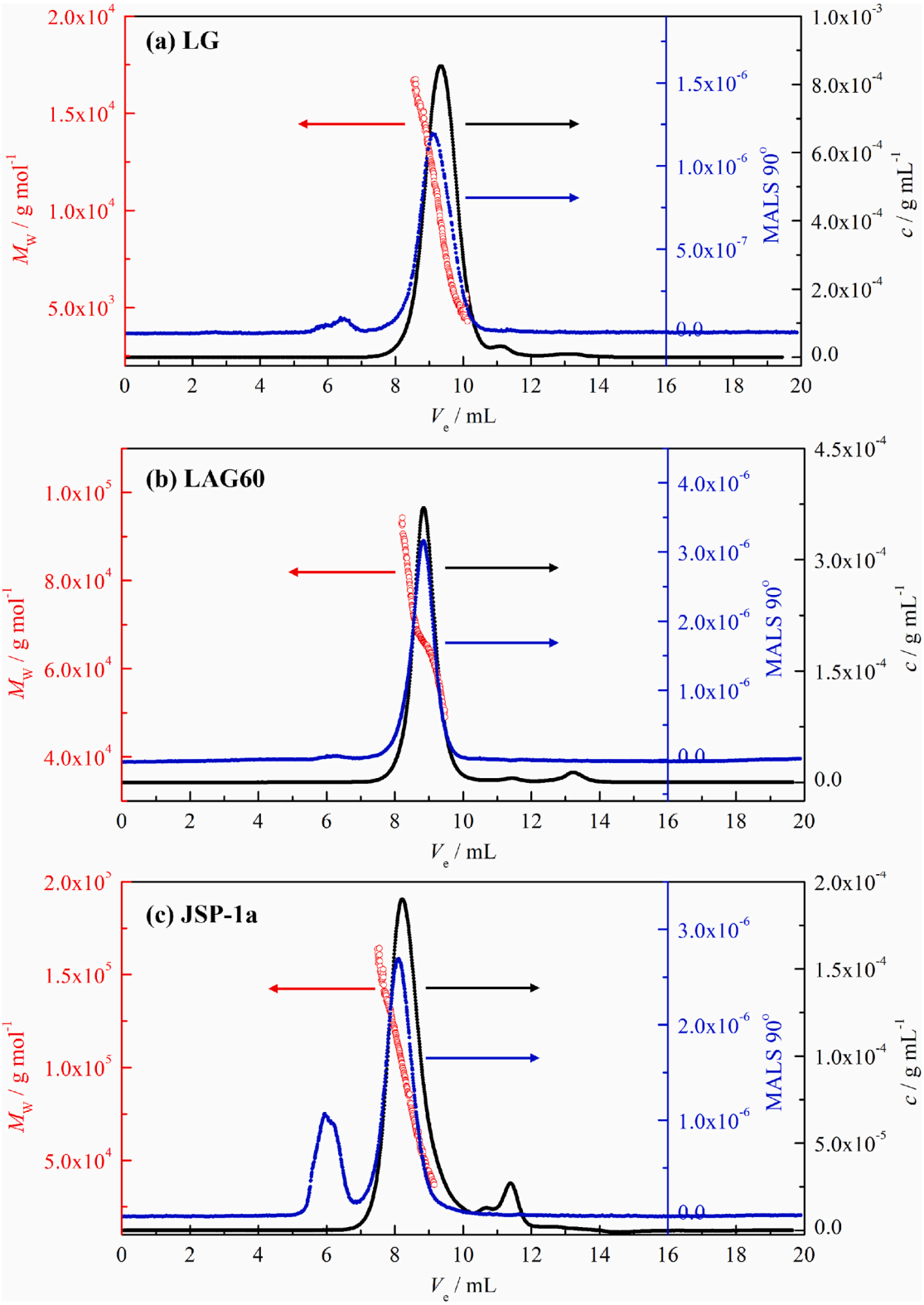

Fig. 1. SEC-MALS profiles of LG (a), LAG60 (b), and JSP-1a (c) in 0.1 M aqueous NaCl.

polysaccharide, in aqueous media (Ioan et al., 1999) at the same M_w, suggesting that LAG60 likely exhibits compact dimensions with a highly branched architecture. The R_g data of JSP-1a in two aqueous solutions are quite comparable to those of an intermediately branched polysaccharide from the sclerotia of *Pleurotus tuber-regium* (Tao et al., 2007), and noticeably smaller than those of dextran with a low degree of branching (Ioan et al., 2000). This indicates that JSP-1a has a hyperbranched structure with intermediate compactness compared to that of larch wood arabinogalactan.

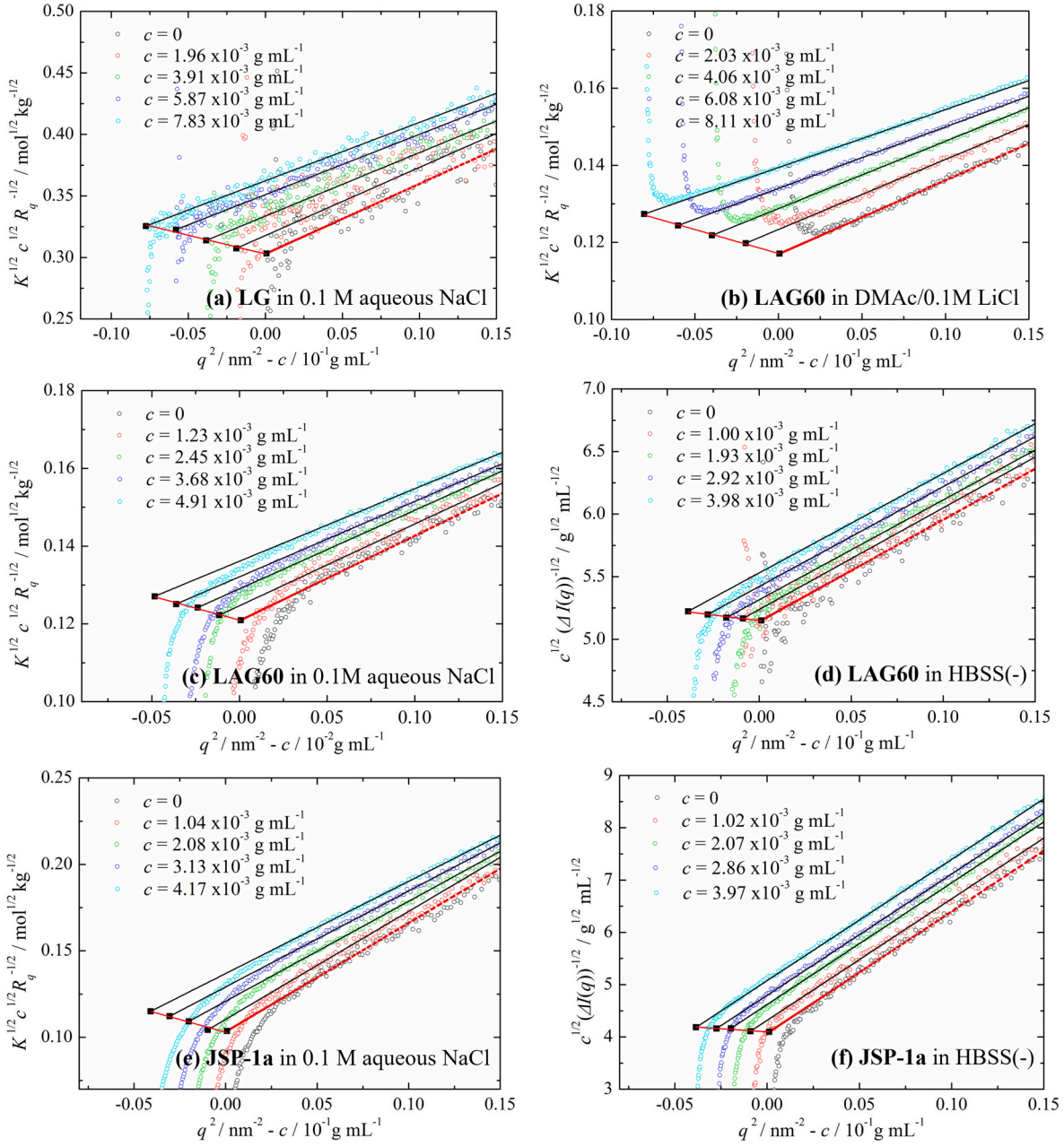

Fig. 2. Berry plots of LG in 0.1 M aqueous NaCl (a), LAG60 in DMAc/0.1 M LiCl (b), LAG60 in 0.1 M aqueous NaCl (c), LAG60 in HBSS(−) (d), JSP-1a in 0.1 M aqueous NaCl (e), and JSP-1a in HBSS(−) (f) at 25 °C.

3.3. *Branching structures deduced from SAXS data*

The angular dependence of the scattering intensity in the higher q range reflects the branching structure of polymer chain in solution. As illustrated in Fig. 4, the distinct slopes in the double-logarithmic SAXS plots indicate differences in the branching architectures of the three AGs. The slope of LG in 0.1 M aqueous NaCl is −1.4 when $qR_g > 3$, which lies between the theoretical values of a rigid rod (−1) and a Gaussian chain (−2), which is also typical of a wormlike chain. The slope of LAG60 in different media is −2.5 when $2.4 < qR_g < 4.5$, but decreases further when $qR_g > 4.5$. When $3 < qR_g < 6$, JSP-1a exhibits slopes of −2.1 and − 2.5 in 0.1 M aqueous NaCl and HBSS(−), respectively. These values for the latter two arabinogalactans are characteristic of hyper-branched polymers (Kishimoto et al., 2022).

Since LG does not have appreciable chain branching, the $P(q)$ data for LG were modeled by the wormlike chain. When the chain thickness is considered as the touched bead with diameter d_b, $P(q)$ is expressed as following equation (Burchard & Kajiwara, 1970; Nakamura & Norisuye, 2004).

$$P(q) = \left[3\left(\frac{2}{qd_b}\right)^3\left(\sin\frac{qd_b}{2} - \frac{qd_b}{2}\cos\frac{qd_b}{2}\right)\right]^2 P_0(q) \quad (4)$$

where $P_0(q)$ is the form factor of an infinitely thin wormlike chain, as proposed by Yoshizaki and Yamakawa (1980). $P_0(q)$ can be calculated as a function of q with the wormlike chain parameters of the contour length L and Kuhn segment length L_K, a measure of the chain stiffness. A curve-fitting procedure was applied to the data of LG presented in Fig. 5(a) to estimate the parameters, L, L_K, and d_b, which are summarized in Table 3. The third parameter d_b was estimated to be 0. This is reasonable because d_b from the SAXS measurement reflects the electron density profile of the chain cross section including solvent molecules surrounding the

Table 2
Results of molecular properties from SAXS and DLS.

	Solvent	LG	LAG60	JSP-1a
M_w/kg mol^{-1}	0.1 M aq. NaCl	10.9	68.5	93.9
	DMAc/0.1 M LiCl	–	73.1	–
A_2/10^{-4} mol cm^3 g^{-1}	0.1 M aq. NaCl	9.40	1.50	3.25
	HBSS(−)	–	2.71	2.45
	DMAc/0.1 M LiCl	–	1.59	–
R_g[a]/nm	0.1 M aq. NaCl	3.37 ± 0.07	3.30 ± 0.06	6.05 ± 0.12
	HBSS(−)	–	3.08 ± 0.21	5.86 ± 0.11
	DMAc/0.1 M LiCl	–	3.12 ± 0.06	–
R_H[b]/nm	0.1 M aq. NaCl	2.33 ± 0.13	3.20 ± 0.24	4.59 ± 0.15
	HBSS(−)	–	3.21 ± 0.04	4.69 ± 0.19
	DMAc/0.1 M LiCl	–	3.34 ± 0.29	–
R_g/R_H	0.1 M aq. NaCl	1.75 ± 0.06	1.03 ± 0.08	1.32 ± 0.04
	HBSS(−)	–	0.96 ± 0.07	1.25 ± 0.13
	DMAc/0.1 M LiCl	–	0.93 ± 0.08	–

[a] From Berry plot of SAXS.
[b] From DLS.

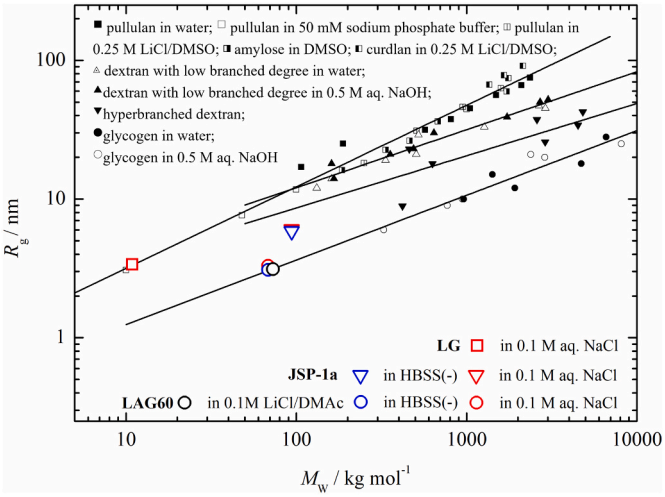

Fig. 3. Double logarithmic plots of gyration radius R_g vs. weight-averaged molar mass M_w for arabinogalactans in different solvents (pullulan in water, 25 °C (Kato et al., 1984); pullulan in 50 mM sodium phosphate buffer, pH 6.9, 24 °C (Watanabe & Inoko, 2011); pullulan in 0.25 M LiCl/DMSO, 25 °C (Tao et al., 2009); amylose in DMSO (Nakanishi et al., 1993); curdlan in 0.25 M LiCl/DMSO, 25 °C (Tao et al., 2009); dextran with low branched degree in water, 20 °C (Ioan et al., 2000); dextran with low branched degree in 0.5 M aq. NaOH, 20 °C (Ioan et al., 2000); hyperbranched dextran, 25 °C (Tao et al., 2007); glycogen in water, 20 °C (Ioan et al., 1999); glycogen in 0.5 M aq. NaOH, 20 °C (Ioan et al., 1999)).

polymer chain (Jiang et al., 2017; Ryoki et al., 2018). The radius of gyration of the wormlike chain can be calculated by the following Benoit-Doty equation:

$$R_g^2 = \frac{LL_K}{6} - \frac{{L_K}^2}{4} + \frac{{L_K}^3}{4L} - \frac{{L_K}^4}{8L^2}\left(1 - e^{-2L/L_K}\right) \quad (5)$$

The calculated R_g = 3.40 nm is reasonably close to that estimated from the Berry plot (3.37 nm). The estimated L_K was 2.80 nm, which is

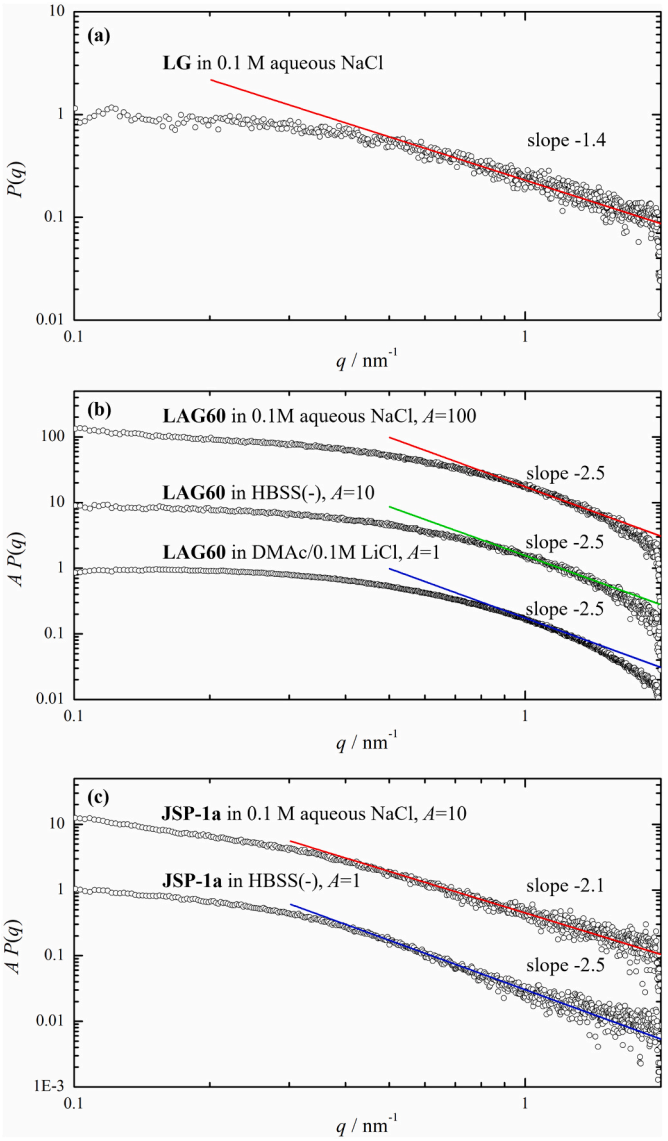

Fig. 4. Double logarithmic plots of the form factor $P(q)$ vs q for LG (a), LAG60 (b), and JSP-1a (c) in indicated solvents at 25 °C.

smaller than that of amylose in ionic liquid (3.50 nm) (Jiang et al., 2017), amylose in DMSO (4.00 nm) (Nakanishi et al., 1993), and xyloglucan in water (16 nm) (Muller et al., 2011), indicating that LG possessed a more flexible chain. It should be noted that we did not consider intramolecular excluded-volume effects on the analysis of $P(q)$ and R_g. This is reasonable because the Kuhn segment number N_K = 7 defined as L/L_K is substantially smaller than 20–50, which is the threshold where the excluded volume effects on R_g is appreciable (Norisuye et al., 1996; Norisuye & Fujita, 1982). It is consistent with the calculation of $P(q)$ (Pedersen & Schurtenberger, 1996).

On the other hand, the estimated M_L value for LG was 0.505 kg mol^{-1} nm^{-1}, which is consistent with the chemical structure discussed in Section 3.1, indicating that LG is unlikely to have a branching structure. The M_L value also yielded the contour length h per glycosidic residue (=M_0/M_L) of 0.33 nm. This value is reasonable, it reflects the local helical structure as well as hydrophobic interactions (Nakanishi et al., 1993; Terao & Sato, 2018; Tomofuji et al., 2019).

As described in Section 3.1, JSP-1a and LAG60 have numerous branching points within a single molecule. Burchard et al. proposed a Gaussian-based hyperbranched chain model (Burchard, 1972), which was subsequently extended to include the intramolecular excluded

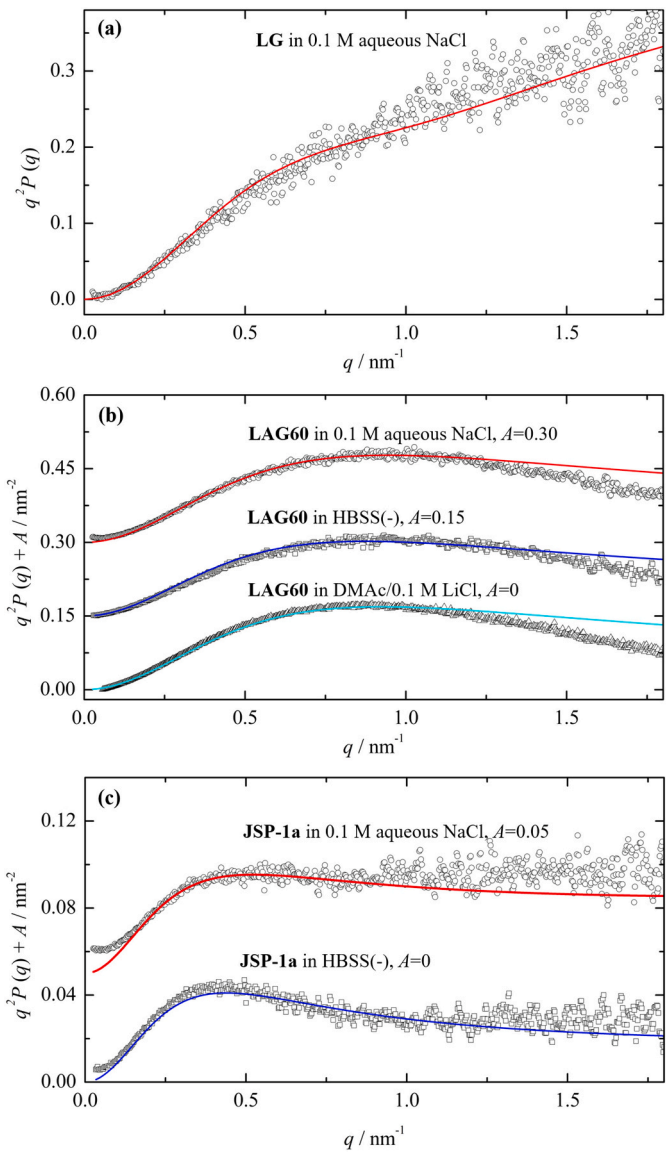

Fig. 5. Kratky plot of LG (a), LAG60 (b), and JSP-1a (c) in the indicated solvents at 25 °C.

Table 3
Wormlike chain parameters for LG in 0.1 M aqueous NaCl.

L/nm	L_K/nm	d_b/nm	M_L/kg mol^{-1} nm^{-1}	h/nm
20.0	2.80	0	0.505	0.33

volume effect for polymers in good solvents (Burchard, 2004; Lederer & Burchard, 2015), taking into account the fractal dimensions of the partial chains. We recently demonstrated that this model is applicable to the highly branched polysaccharide derivatives with various main chain stiffness (Kishimoto et al., 2022; Kobayashi & Terao, 2024; Mizuguchi et al., 2023). The form factor $P(u)$ for the perturbed wormlike chain can be written as a function of u ($\equiv q\,R_{g,HB}$) to be

$$P(u) = \left[\frac{\sin[(d-1)\arctan(\xi_{br}u)]}{(d-1)(\xi_{br}u)\left(1+\xi_{br}{}^2u^2\right)^{(d-1)/2}}\right]^2 \Bigg/ \left[\frac{\sin[(d-1)\arctan(\xi_{lin}u)]}{(d-1)(\xi_{lin}u)\left(1+\xi_{lin}{}^2u^2\right)^{(d-1)/2}}\right] \quad (6)$$

with

$$\xi_{br}{}^2 = \frac{C+1}{d(d+1)} \quad (7)$$

$$\xi_{lin}{}^2 = \frac{2C}{d(d+1)} \quad (8)$$

where $1/C$ represents the number of branching points per polysaccharide molecule, and d is the fractal dimension of the linear chain. The d value is 2.0 for unperturbed Gaussian chains, and $d = 1.7$ is that with the intramolecular excluded volume effect.

Theoretical fitting of the Kratky plots for LAG60 in three solvents (Fig. 5(b)) was performed using the hyperbranched chain model, and the $1/C$ value was estimated to be 130 based on the NMR results. However, the theoretical values calculated using this $1/C$ value could not reproduce the experimental data, regardless of the combination of $R_{g,HB}$ and d, even when d was varied within a plausible range of 1.7 to 2.0. When the $1/C$ value was adjusted to 96, which was calculated under the condition that single galactose branches were excluded, the theoretical values agree with the experimental data in the q range between 0.1 nm^{-1} and 1 nm^{-1}, and the resulting parameters are summarized in Table 4. A possible explanation for this discrepancy in the $1/C$ value is that the SAXS conditions used were not sufficient to distinguish the scattering contribution of single-sugar-residue side chains from that of the main chain. Nevertheless, the resulting $R_{g,HB}$ is consistent with that from the Berry plot, and $d = 1.7$ indicates that these are good solvent systems. As q increases beyond 1 nm^{-1}, the discrepancy between the theoretical curve and the experimental data becomes significant. This deviation is likely due to the local structure of the polymer, and is consistent with previous comparisons between experimental and theoretical values (Burchard et al., 2012; Kishimoto et al., 2022).

Since there were uncertainties in the structures of JSP-1a, the arrangement of its primary structure and the estimation of the number of branch points could be informed by the analysis of LAG60. In previous research, the linkage between terminal arabinose residues and the backbone and the linkage between terminal arabinose and 1,5-β-arabinose were confirmed by various analytical techniques. After excluding the contribution of single terminal arabinose residues based on the previously proposed primary structure (Huang et al., 2023), the number of branching points on the JSP-1a backbone was $1/C = 50$. We therefore analyzed the $P(q)$ data using Eqs. (6)–(8). Unfortunately, this $1/C$ value did not yield suitable fitting results. We then explored an alternative structural model by rearranging the possible branching structure to a hexasaccharide substituting 8 % of the galactose of the main chain as shown in Fig. S4(D), the $1/C$ of this primary structure was reduced to 25, which resulted in suitable $R_{g,HB}$ that were consistent with the experimental data, and this model provided a good fit to the Kratky plot. The fitting parameters evaluated are listed in Table 4. As displayed in Fig. 5 (c), there were also some deviations of experimental data from model fitting curves. In the low-q region, where q is smaller than 0.2 nm^{-1}, this is due to the aggregation of JSP-1a, while in the q region above 1 nm^{-1}, the deviations are attributed to the local structure of JSP-1a as was the case for LAG60.

3.4. Hydrodynamic properties in diluted solution

The ratio of R_g/R_H from the same polysaccharide-solvent system can be used to predict or examine the architecture of the polymer if its

Table 4
Molecular parameters for LAG60 and JSP-1a at 25 °C.

	LAG60			JSP-1a	
	in 0.1 M aq. NaCl	in HBSS (−)	in DMAc/0.1 M LiCl	in 0.1 M aq. NaCl	in HBSS (−)
R_g[a]/nm	3.30 ± 0.06	3.08 ± 0.21	3.12 ± 0.06	6.05 ± 0.12	5.87 ± 0.11
$R_{g,HB}$/nm	3.10	3.35	3.18	6.30	6.30
1/C	96	96	96	25	25
d	1.7	1.7	1.7	1.7	1.9

[a] From Berry plot of SAXS.

Table 5
Hydrodynamic properties of the three arabinogalactan samples at 25.0 °C.

Sample	LG	LAG60	JSP-1a
$[\eta]$/mL g^{-1}	9.50	5.08	14.26
k'	0.41	0.55	0.69
$\Phi/10^{23}$ mol^{-1}	1.70	6.42	4.42
$A_2 M_w/[\eta]$	1.01	2.02	2.14

polydispersity is not significantly high (Burchard, 1999). Here, the R_g data obtained from SAXS were used instead of those obtained from SLS, while the hydrodynamic radii R_H were determined from the fast moiety data of the intensity-weighted distributions (Fig. S6). According to SEC results, our samples showed low to moderate polydispersity ($Đ$ = 1.03–1.21, Table 1), while DLS results indicated the presence of aggregates in aqueous solutions (Fig. S6). It should be noted that this proportion is actually low, but appears more pronounced in the intensity-weighted distributions. These factors may slightly affect the absolute R_g/R_H values. When dissolved in 0.1 M aqueous NaCl, LG exhibited a ratio of 1.75, which was close to the theoretical value for a monodisperse linear Gaussian chain in good solvent (1.78) (Burchard, 1999). The R_g/R_H ratios of LAG60 in all three media were around 1.0, lying between those of the dendrimer (0.977) and the hyperbranched polymer (1.225) (Burchard, 1999). The corresponding ratios of JSP-1a in aqueous media ranged from 1.25 to 1.32 which was close to the typical value for hyperbranched polymer (1.225). Since the primary structure of LAG60 does not follow a dendrimer structure, both LAG60 and JSP-1a are considered to have a hyperbranched structures, with LAG60 adopting a more compact.

The Mead-Fuoss plot and the Huggins plot of each sample are shown in Fig. S8. The Mead-Fuoss plot exhibited better linearity, particularly for the branched polysaccharide samples, likely due to the high Huggins constant k'. The intrinsic viscosity $[\eta]$ determined from the common intercept and k' estimated from the Mead-Fuoss plot are summarized in Table 5. Notably, the Huggins coefficient k' determined from both plots was roughly consistent. Taking into consideration that a high k' is often observed for branched polysaccharide derivatives (Kishimoto et al., 2022) and the other synthetic branched polymers (Hokajo et al., 2001; Terao et al., 1999) in good solvents, the current results are reasonable for linear and branched polysaccharides in good solvent systems.

The reduced hydrodynamic volume Φ, also known as the Flory viscosity factor and defined by Eq. (9), is generally related to the shape of the polymer in solution. This parameter is particularly useful when only single-point M_w data are available, as it enables comparison of polymer compactness across samples with different conformations.

$$\Phi = \frac{[\eta]M_w}{6^{3/2}R_g^3} \tag{9}$$

The Φ value of LG is smaller than that of typical linear flexible polymers (2.5–2.8 × 10^{23} mol^{-1}), which is probably attributed to the higher chain stiffness of LG. However, it is still larger than the Φ value reported for xyloglucan in water (8.02 × 10^{22} mol^{-1}) (Muller et al., 2011) or konjac glucomannan in water (3.67–9.44 × 10^{22} mol^{-1}) (Guo, Yokoyama, et al., 2021), likely due to the higher chain stiffness of LG. On the other hand, the Φ values of LAG60 and JSP-1a are intermediate between the theoretical values for a hard sphere (9.23 × 10^{23} mol^{-1}) and a linear chain (1.95 × 10^{22} mol^{-1}). The Φ value of LAG60 and JSP-1a is relatively higher than that of some hyperbranched polymers, such as hydroxyethyl amylopectin in pure water (2.97 × 10^{23} mol^{-1}) (Sarazin et al., 1992), highly branched cyclic dextrin tris(phenylcarbamate) in 1,4-dioxane (3.44 × 10^{23} mol^{-1}) and in methyl acetate (3.77 × 10^{23}

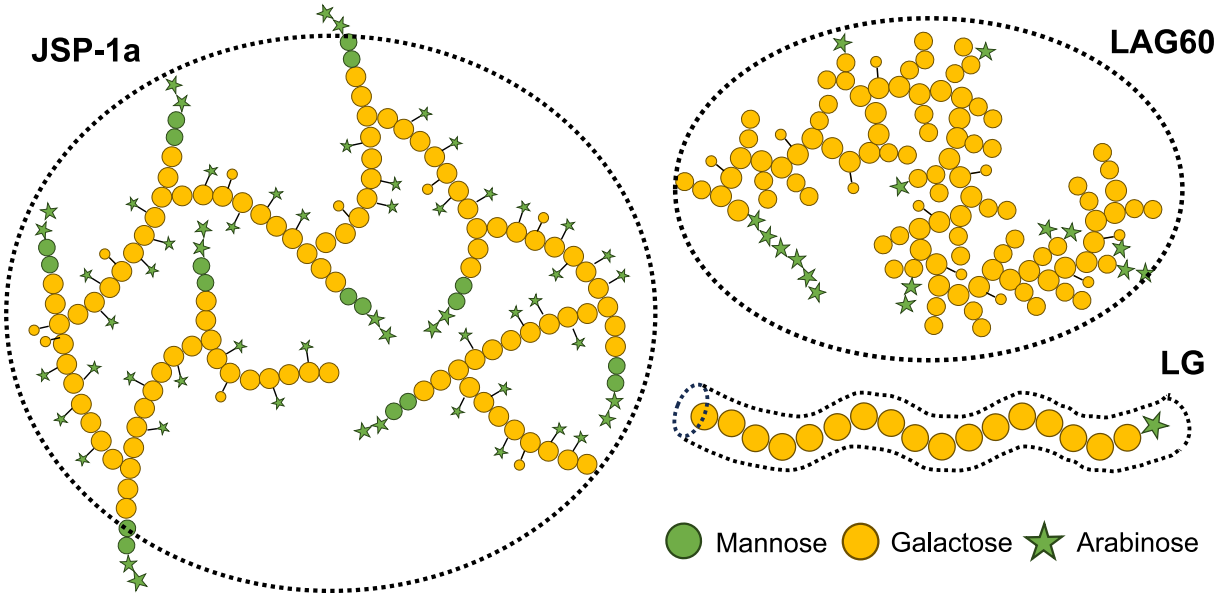

Fig. 6. Schematic representation for wormlike chain structure of LG and hyperbranched structure of LAG60 and JSP-1a.

mol^{-1}) (Mizuguchi et al., 2023), as well as highly branched cyclic dextrin tris(3,5-dimethylphenylcarbamate) in methyl acetate (2.27 × 10^{23} mol^{-1}) and in 4-methyl-2-pentanone (2.44 × 10^{23} mol^{-1}) (Kishimoto et al., 2022). This may result from the higher flexibility of the 1,3-linked or 1,6-linked galactan chains, which contribute to a higher apparent polymer segment density.

The differences in the dimensional and hydrodynamic properties of the three arabinogalactans can also be analyzed in terms of the ratio of A_2M_w to $[\eta]$, which is derived from the overlap concentrations defined by A_2 and $[\eta]$, respectively (Galinsky & Burchard, 1996). The ratio $A_2M_w/[\eta]$ for LG was calculated to be 1.01, which fell within the range of values (0.98–1.23) reported for linear amylose in DMSO with low molar mass (18.9–464 kg mol^{-1}) (Nakanishi et al., 1993). In contrast, significantly higher $A_2M_w/[\eta]$ values of 2.02 and 2.14 were found for LAG60 and JSP-1a, respectively. These values are consistent with the range of 2.0–2.4 observed for hyperbranched polymers, including amylopectin in pure water (Galinsky & Burchard, 1996) and some low M_w glycogen (326–945 kg mol^{-1}) in aqueous sodium hydroxide solution (Ioan et al., 1999). Based on the above results, LG is proposed to adopt a linear wormlike chain structure, while LAG60 and JSP-1a exhibit hyperbranched structures, as illustrated in Fig. 6. In this systematic representation, LAG60 adopts a more compact conformation compared to JSP-1a.

4. Conclusions

Three arabinogalactans with different backbone linkages and branching structures were characterized using SAXS, DLS, and viscosity measurements. The linear arabinogalactan LG was well described by the infinite thin wormlike chain model with a relatively low Kuhn segment length of 2.80 nm, a value comparable to that of amylose in some solvents. In contrast, the branched arabinogalactans, LAG60 and JSP-1a, were modeled using a perturbed hyperbranched chain model under specific conditions: (1) branching points were defined such that branches consisting of only a single sugar residue were excluded; and (2) a refined hexasaccharide-level branching structure was assumed for JSP-1a. The conformational properties of the three arabinogalactans were further supported by analysis of the Flory viscosity factor Φ, the ratio of R_g/R_H, and $A_2M_w/[\eta]$. This work provides insights into the conformational details of linear and branched arabinogalactans.

CRediT authorship contribution statement

Hai Huang: Writing – review & editing, Writing – original draft, Investigation, Formal analysis, Data curation, Conceptualization. **Mengqi Wu:** Writing – review & editing, Supervision, Resources. **Rintaro Takahashi:** Writing – review & editing, Supervision. **Wenqing Zhang:** Writing – review & editing, Supervision, Resources, Conceptualization. **Ken Terao:** Writing – review & editing, Supervision, Funding acquisition, Conceptualization.

Declaration of competing interest

The authors declare the following financial interests/personal relationships which may be considered as potential competing interests: Ken Terao reports financial support was provided by Japan Society for the Promotion of Science. If there are other authors, they declare that they have no known competing financial interests or personal relationships that could have appeared to influence the work reported in this paper.

Acknowledgments

The authors are grateful to Dr. Noboru Ohta (SPring-8) for the SAXS measurements. The synchrotron radiation experiments were performed at the BL40B2 in SPring-8 with the approval of the Japan Synchrotron Radiation Research Institute (JASRI) (proposal Nos. 2023A1111, 2023A1112, 2023B1124, 2023B1125, 2024A1118, 2024A1119, 2024B1152, and 2024B1153). The NMR and CHN analysis measurements were performed at Analytical Instrument Facility, Graduate School of Science, The University of Osaka. This work was partially supported by JSPS KAKENHI grant Nos. JP23H02011 and JP23K26704.

Appendix A. Supplementary data

Additional table for chemical component of AGs, and additional figures for SAXS, HPLC, NMR, primary structures, DLS, SLS, and viscometry. Supplementary data to this article can be found online at https://doi.org/10.1016/j.carbpol.2025.124371.

Data availability

Data will be made available on request.

References

Bradford, M. M. (1976). A rapid and sensitive method for the quantitation of microgram quantities of protein utilizing the principle of protein-dye binding. *Analytical Biochemistry, 72*, 248–254. https://doi.org/10.1016/0003-2697(76)90527-3

Brecker, L., Wicklein, D., Moll, H., Fuchs, E. C., Becker, W. M., & Petersen, A. (2005). Structural and immunological properties of arabinogalactan polysaccharides from pollen of timothy grass (Phleum pratense L.). *Carbohydrate Research, 340*, 657–663. https://doi.org/10.1016/j.carres.2005.01.006

Burchard, W. (1972). Angular-distribution of Rayleigh-scattering from branched polycondensates - amylopectin and glycogen types. *Macromolecules, 5*, 604. https://doi.org/10.1021/ma60029a015

Burchard, W. (1999). Solution properties of branched macromolecules. In J. Roovers (Ed.), *Branched polymers II* (pp. 113–194). Berlin, Heidelberg: Springer Berlin Heidelberg. https://doi.org/10.1007/3-540-49780-3_3.

Burchard, W. (2004). Angular dependence of scattered light from hyperbranched structures in a good solvent. A fractal approach. *Macromolecules, 37*, 3841–3849. https://doi.org/10.1021/ma049950l

Burchard, W., & Kajiwara, K. (1970). The statistics of stiff chain molecules I. The particle scattering factor. *Proceedings of the Royal Society of London. Series A: Mathematical and Physical Sciences, 316*, 185–199. https://doi.org/10.1098/rspa.1970.0074

Burchard, W., Khalyavina, A., Lindner, P., Schweins, R., Friedel, P., Wiemann, M., & Lederer, A. (2012). SANS investigation of global and segmental structures of hyperbranched aliphatic-aromatic polyesters. *Macromolecules, 45*, 3177–3187. https://doi.org/10.1021/ma300031g

Cheng, J., Wei, C., Li, W., Wang, Y., Wang, S., Huang, Q., Liu, Y., & He, L. (2021). Structural characteristics and enhanced biological activities of partially degraded arabinogalactan from larch sawdust. *International Journal of Biological Macromolecules, 171*, 550–559. https://doi.org/10.1016/j.ijbiomac.2021.01.039

de Oliveira, A. J., Cordeiro, L. M., Goncalves, R. A., Ceole, L. F., Ueda-Nakamura, T., & Iacomini, M. (2013). Structure and antiviral activity of arabinogalactan with (1–>6)-beta-D-galactan core from *Stevia rebaudiana* leaves. *Carbohydrate Polymers, 94*, 179–184. https://doi.org/10.1016/j.carbpol.2012.12.068

Dror, Y., Cohen, Y., & Yerushalmi-Rozen, R. (2006). Structure of gum arabic in aqueous solution. *Journal of Polymer Science Part B: Polymer Physics, 44*, 3265–3271. https://doi.org/10.1002/polb.20970

Galinsky, G., & Burchard, W. (1996). Starch fractions as examples for nonrandomly branched macromolecules .2. Behavior in the semidilute region. *Macromolecules, 29*, 1498–1506. https://doi.org/10.1021/ma9513527

Glatter, O., & Kratky, O. (1982). *Small angle X-ray scattering*. London: Academic Press.

Goellner, E. M., Utermoehlen, J., Kramer, R., & Classen, B. (2011). Structure of arabinogalactan from Larix laricina and its reactivity with antibodies directed against type-II-arabinogalactans. *Carbohydrate Polymers, 86*, 1739–1744. https://doi.org/10.1016/j.carbpol.2011.07.006

Guo, L. P., Yokoyama, W., Chen, L., Liu, F., Chen, M. S., & Zhong, F. (2021). Characterization and physicochemical properties analysis of konjac glucomannan: Implications for structure-properties relationships. *Food Hydrocolloids, 120*, Article 106818. https://doi.org/10.1016/j.foodhyd.2021.106818

Guo, W., Rao, G., & Wen, X. (2021). Arabinogalactan in banana: Chemical characterization and pharmaceutical effects. *International Journal of Biological Macromolecules, 167*, 1059–1065. https://doi.org/10.1016/j.ijbiomac.2020.11.060

He, F., Zhang, S., Li, Y., Chen, X., Du, Z., Shao, C., & Ding, K. (2021). The structure elucidation of novel arabinogalactan LRP1-S2 against pancreatic cancer cells growth in vitro and in vivo. *Carbohydrate Polymers, 267*, Article 118172. https://doi.org/10.1016/j.carbpol.2021.118172

He, T.-B., Huang, Y.-P., Huang, Y., Wang, X.-J., Hu, J.-M., & Sheng, J. (2018). Structural elucidation and antioxidant activity of an arabinogalactan from the leaves of Moringa oleifera. *International Journal of Biological Macromolecules, 112*, 126–133. https://doi.org/10.1016/j.ijbiomac.2018.01.110

Hinz, S. W., Verhoef, R., Schols, H. A., Vincken, J. P., & Voragen, A. G. (2005). Type I arabinogalactan contains beta-D-Galp-(1–>3)-beta-D-Galp structural elements.

Carbohydrate Research, 340, 2135–2143. https://doi.org/10.1016/j.carres.2005.07.003
Hokajo, T., Terao, K., Nakamura, Y., & Norisuye, T. (2001). Solution properties of polymacromonomers consisting of polystyrene - V. Effect of side chain length on chain stiffness. *Polymer Journal, 33*, 481–485. https://doi.org/10.1295/polymj.33.481
Huang, H., Yang, X., Li, W., Han, Q., Xu, Z., Xia, W., Wu, M., & Zhang, W. (2023). Structural characterization and immunomodulatory activity of an arabinogalactan from Jasminum sambac (L.) Aiton tea processing waste. *International Journal of Biological Macromolecules, 235*, Article 123816. https://doi.org/10.1016/j.ijbiomac.2023.123816
Huang, W., Xie, Y., Guo, T., Dai, W., Nan, L., Wang, Q., Liu, Y., Lan, W., Wang, Z., Huang, L., & Gong, G. (2024). A new perspective on structural characterisation and immunomodulatory activity of arabinogalactan in Larix kaempferi from Qinling Mountains. *International Journal of Biological Macromolecules, 265*, Article 130859. https://doi.org/10.1016/j.ijbiomac.2024.130859
Ioan, C. E., Aberle, T., & Burchard, W. (1999). Solution properties of glycogen. 1. Dilute solutions. *Macromolecules, 32*, 7444–7453. https://doi.org/10.1021/ma990600m
Ioan, C. E., Aberle, T., & Burchard, W. (2000). Structure properties of dextran. 2. Dilute solution. *Macromolecules, 33*, 5730–5739. https://doi.org/10.1021/ma000282n
Jiang, X. Y., Kitamura, S., Sato, T., & Terao, K. (2017). Chain dimensions and stiffness of cellulosic and amylosic chains in an ionic liquid: Cellulose, amylose, and an amylose carbamate in BmimCl. *Macromolecules, 50*, 3979–3985. https://doi.org/10.1021/acs.macromol.7b00389
Jinbo, Y., Teranuma, O., Kanao, M., Sato, T., & Teramoto, A. (2003). Light-scattering study of semiflexible polymer solutions. 4. n-hexane solutions of poly(n-hexyl isocyanate). *Macromolecules, 36*, 198–203. https://doi.org/10.1021/ma020704o
Kato, T., Katsuki, T., & Takahashi, A. (1984). Static and dynamic properties of pullulan in a dilute-solution. *Macromolecules, 17*, 1726–1730. https://doi.org/10.1021/ma00139a016
Kishimoto, A., Mizuguchi, M., Ryoki, A., & Terao, K. (2022). Molecular structure and chiral recognition ability of highly branched cyclic dextrin carbamate derivative. *Carbohydrate Polymers, 290*, Article 119491. https://doi.org/10.1016/j.carbpol.2022.119491
Kobayashi, A., & Terao, K. (2024). Highly branched thermoresponsive polysaccharide derivative in water. Partly substituted highly branched cyclic dextrin ethylcarbamate. *Carbohydrate Polymers, 343*, Article 122473. https://doi.org/10.1016/j.carbpol.2024.122473
Lederer, A., & Burchard, W. (2015). *Hyperbranched polymers: Macromolecules in between deterministic linear chains and dendrimer structures (polymer chemistry series vol. 16)*. Royal Society of Chemistry. https://doi.org/10.1039/9781782622468
Li, H., Gao, T., Zhang, Z., Lei, J., Hu, J., Tang, Z., … Yuan, M. (2023). A novel Stauntonia leucantha fruits arabinogalactan: And structural characterization. *Carbohydrate Polymers, 303*, Article 120481. https://doi.org/10.1016/j.carbpol.2022.120481
Liang, F., Hu, C., He, Z., & Pan, Y. (2014). An arabinogalactan from flowers of Chrysanthemum morifolium: Structural and bioactivity studies. *Carbohydrate Research, 387*, 37–41. https://doi.org/10.1016/j.carres.2013.09.002
Loosveld, A. M. A., Grobet, P. J., & Delcour, J. A. (1997). Contents and structural features of water-extractable arabinogalactan in wheat flour fractions. *Journal of Agricultural and Food Chemistry, 45*, 1998–2002. https://doi.org/10.1021/jf960901k
Mikhailenko, M. A., Sharafutdinov, M. R., Kozlov, A. S., Kuznetsova, S. A., Shakhtshneider, T. P., & Zolotarev, K. V. (2016). Study of arabinogalactan supramolecular structure using synchrotron radiation SAXS and terahertz laser ablation methods. In *, 84. Proceedings of the international conference synchrotron and free electron laser radiation: Generation and application (SFR-2016)* (pp. 382–385). https://doi.org/10.1016/j.phpro.2016.11.065
Mizuguchi, M., Umeda, K., Mizumoto, H., & Terao, K. (2023). Solution characterization of a hyperbranched polysaccharide carbamate derivative and specific phase separation behavior due to chain branching. *Soft Matter, 19*, 7781–7786. https://doi.org/10.1039/d3sm01074k
Mora-Gutierrez, A., Attaie, R., Nunez de Gonzalez, M. T., Jung, Y., Woldesenbet, S., & Marquez, S. A. (2018). Complexes of lutein with bovine and caprine caseins and their impact on lutein chemical stability in emulsion systems: Effect of arabinogalactan. *Journal of Dairy Science, 101*, 18–27. https://doi.org/10.3168/jds.2017-13105
Muller, F., Manet, S., Jean, B., Chambat, G., Boue, F., Heux, L., & Cousin, F. (2011). SANS measurements of semiflexible xyloglucan polysaccharide chains in water reveal their self-avoiding statistics. *Biomacromolecules, 12*, 3330–3336. https://doi.org/10.1021/bm200881x
Nakamura, Y., & Norisuye, T. (2004). Scattering function for wormlike chains with finite thickness. *Journal of Polymer Science Part B: Polymer Physics, 42*, 1398–1407. https://doi.org/10.1002/polb.20026
Nakanishi, Y., Norisuye, T., Teramoto, A., & Kitamura, S. (1993). Conformation of amylose in dimethyl-sulfoxide. *Macromolecules, 26*, 4220–4225. https://doi.org/10.1021/Ma00068a023
Nakata, Y., Kitamura, S., & Terao, K. (2024). Dual thermoresponsive polysaccharide derivative – Water system. Partially substituted amylose butylcarbamate in water. *Carbohydrate Polymers, 325*, Article 121587. https://doi.org/10.1016/j.carbpol.2023.121587
Norisuye, T., & Fujita, H. (1982). Excluded-volume effects in dilute polymer solutions. XIII. Effects of chain stiffness. *Polymer Journal, 14*, 143–147. https://doi.org/10.1295/polymj.14.143
Norisuye, T., Tsuboi, A., & Teramoto, A. (1996). Remarks on excluded-volume effects in semiflexible polymer solutions. *Polymer Journal, 28*, 357–361. https://doi.org/10.1295/polymj.28.357
Pedersen, J. S., & Schurtenberger, P. (1996). Scattering functions of semiflexible polymers with and without excluded volume effects. *Macromolecules, 29*, 7602–7612. https://doi.org/10.1021/Ma9607630
Peng, Q., Liu, H., Lei, H., & Wang, X. (2016). Relationship between structure and immunological activity of an arabinogalactan from Lycium ruthenicum. *Food Chemistry, 194*, 595–600. https://doi.org/10.1016/j.foodchem.2015.08.087
Ponder, G. R. (1998). Arabinogalactan from western larch. Part IV. Polymeric products of partial acid hydrolysis. *Carbohydrate Polymers, 36*, 1–14. https://doi.org/10.1016/S0144-8617(98)00014-9
Ponder, G. R., & Richards, G. N. (1997). Arabinogalactan from Western larch, part III: Alkaline degradation revisited, with novel conclusions on molecular structure. *Carbohydrate Polymers, 34*, 251–261. https://doi.org/10.1016/s0144-8617(97)00099-4
Qin, F., Sletmoen, M., Stokke, B. T., & Christensen, B. E. (2013). Higher order structures of a bioactive, water-soluble (1–>3)-beta-D-glucan derived from *Saccharomyces cerevisiae*. *Carbohydrate Polymers, 92*, 1026–1032. https://doi.org/10.1016/j.carbpol.2012.10.013
Quach, T. T. M., Nguyen, N. T., Yuguchi, Y., Dang, L. V., Van Ngo, Q., & Thanh, T. T. T. (2024). Structure, anticoagulant and cytotoxic activity of a sulfated polysaccharide from green seaweed Chaetomorpha linum. *Natural Product Research, 38*, 555–562. https://doi.org/10.1080/14786419.2023.2180506
Rakhmanberdyeva, R. K., Shashkov, A. S., Bobakulov, K. M., Azizov, D. Z., Malikova, M. K., & Ogay, D. K. (2021). The structure and prebiotic activity of arabinogalactan from Ferula Kuhistsmall a, Cyrillicnica. *Carbohydrate Research, 505*, Article 108342. https://doi.org/10.1016/j.carres.2021.108342
Renard, D., Lepvrier, E., Garnier, C., Roblin, P., Nigen, M., & Sanchez, C. (2014). Structure of glycoproteins from Acacia gum: An assembly of ring-like glycoproteins modules. *Carbohydrate Polymers, 99*, 736–747. https://doi.org/10.1016/j.carbpol.2013.08.090
Ryoki, A., Kim, D., Kitamura, S., & Terao, K. (2018). Linear and cyclic amylose derivatives having brush like side groups in solution: Amylose tris(n-octadecylcarbamate)s. *Polymer, 137*, 13–21. https://doi.org/10.1016/j.polymer.2017.12.063
Saeidy, S., Petera, B., Pierre, G., Fenoradosoa, T. A., Djomdi, D., Michaud, P., & Delattre, C. (2021). Plants arabinogalactans: From structures to physico-chemical and biological properties. *Biotechnology Advances, 53*, Article 107771. https://doi.org/10.1016/j.biotechadv.2021.107771
Sanchez, C., Schmitt, C., Kolodziejczyk, E., Lapp, A., Gaillard, C., & Renard, D. (2008). The acacia gum arabinogalactan fraction is a thin oblate ellipsoid: A new model based on small-angle neutron scattering and ab initio calculation. *Biophysical Journal, 94*, 629–639. https://doi.org/10.1529/biophysj.107.109124
Sarazin, D., Francois, J. H., Verwaerde, C., & Fleche, G. (1992). Structural study of fractionated hydroxyethyl-amylopectin in aqueous-solution. *Journal of Applied Polymer Science, 46*, 715–724. https://doi.org/10.1002/app.1992.070460418
Shimizu, N., Yatabe, K., Nagatani, Y., Saijyo, S., Kosuge, T., & Igarashi, N. (2016). Software development for analysis of small-angle X-ray scattering data. *AIP Conference Proceedings, 1741*, Article 050017. https://doi.org/10.1063/1.4952937
Silva, J., Ferraz, R., Dupree, P., Showalter, A. M., & Coimbra, S. (2020). Three decades of advances in arabinogalactan-protein biosynthesis. *Frontiers in Plant Science, 11*, Article 610377. https://doi.org/10.3389/fpls.2020.610377
Suarez, E. R., Kralovec, J. A., Noseda, M. D., Ewart, H. S., Barrow, C. J., Lumsden, M. D., & Grindley, T. B. (2005). Isolation, characterization and structural determination of a unique type of arabinogalactan from an immunostimulatory extract of Chlorella pyrenoidosa. *Carbohydrate Research, 340*, 1489–1498. https://doi.org/10.1016/j.carres.2005.04.003
Takeuchi, Y., Asano, T., Tsuzaki, K., & Wada, K. (2018). Catalytic asymmetric amination of meso-epoxide using soy polysaccharide (Soyafibe S-DN). *Bulletin of the Chemical Society of Japan, 91*, 678–683. https://doi.org/10.1246/bcsj.20170369
Takeuchi, Y., Asano, T., Tsuzaki, K., Wada, K., & Kurata, H. (2020). Asymmetric amination of meso-epoxide with vegetable powder as a low-toxicity catalyst. *Molecules, 25*, Article 3197. https://doi.org/10.3390/molecules25143197
Tao, Y., Yan, Y., & Xu, W. (2009). Shrinking factors of hyperbranched polysaccharide from fungus. *Carbohydrate Research, 344*, 1311–1318. https://doi.org/10.1016/j.carres.2009.05.004
Tao, Y., Zhang, L., Yan, F., & Wu, X. (2007). Chain conformation of water-insoluble hyperbranched polysaccharide from fungus. *Biomacromolecules, 8*, 2321–2328. https://doi.org/10.1021/bm070335+
Terao, K., Hokajo, T., Nakamura, Y., & Norisuye, T. (1999). Solution properties of polymacromonomers consisting of polystyrene. 3. Viscosity behavior in cyclohexane and toluene. *Macromolecules, 32*, 3690–3694. https://doi.org/10.1021/ma990091o
Terao, K., & Sato, T. (2018). Conformational properties of polysaccharide derivatives. In G. Yang, & L. Lamboni (Eds.), *Bioinspired materials science and engineering* (pp. 167–183). https://doi.org/10.1002/9781119390350.ch9
Tomofuji, Y., Matsuo, K., & Terao, K. (2022). Kinetics of denaturation and renaturation processes of double-stranded helical polysaccharide, xanthan in aqueous sodium chloride. *Carbohydrate Polymers, 275*, Article 118681. https://doi.org/10.1016/j.carbpol.2021.118681
Tomofuji, Y., Yoshiba, K., Christensen, B. E., & Terao, K. (2019). Single-chain conformation of carboxylated schizophyllan, a triple helical polysaccharide, in dilute alkaline aqueous solution. *Polymer, 185*, Article 121944. https://doi.org/10.1016/j.polymer.2019.121944
Villa-Rivera, M. G., Cano-Camacho, H., Lopez-Romero, E., & Zavala-Paramo, M. G. (2021). The role of arabinogalactan type II degradation in plant-microbe interactions. *Frontiers in Microbiology, 12*, Article 730543. https://doi.org/10.3389/fmicb.2021.730543

Wada, K., Asano, Y., Kato, Y., & Hibi, M. (2023). In L. Kyowa Pharma Cchemical Co. (Ed.), *Plant-derived organocatalyst*. Japan Retrieved from https://patentscope2.wipo.int/search/ja/WO2023191088.

Wang, H., Shi, S., Bao, B., Li, X., & Wang, S. (2015). Structure characterization of an arabinogalactan from green tea and its anti-diabetic effect. *Carbohydrate Polymers, 124*, 98–108. https://doi.org/10.1016/j.carbpol.2015.01.070

Watanabe, Y., & Inoko, Y. (2011). Further application of size-exclusion chromatography combined with small-angle X-ray scattering optics for characterization of biological macromolecules. *Analytical and Bioanalytical Chemistry, 399*, 1449–1453. https://doi.org/10.1007/s00216-010-4140-7

Wefers, D., & Bunzel, M. (2016). NMR spectroscopic profiling of arabinan and galactan structural elements. *Journal of Agricultural and Food Chemistry, 64*, 9559–9568. https://doi.org/10.1021/acs.jafc.6b04232

Xu, Y., Dong, Q., Qiu, H., Cong, R., & Ding, K. (2010). Structural characterization of an arabinogalactan from Platycodon grandiflorum roots and antiangiogenic activity of its sulfated derivative. *Biomacromolecules, 11*, 2558–2566. https://doi.org/10.1021/bm100402n

Yao, Y., Yao, J., Du, Z., Wang, P., & Ding, K. (2018). Structural elucidation and immune-enhancing activity of an arabinogalactan from flowers of Carthamus tinctorius L. *Carbohydrate Polymers, 202*, 134–142. https://doi.org/10.1016/j.carbpol.2018.08.098

Yoshizaki, T., & Yamakawa, H. (1980). Scattering functions of wormlike and helical wormlike chains. *Macromolecules, 13*, 1518–1525. https://doi.org/10.1021/ma60078a030

Zhang, C. Q., Chen, X., & Ding, K. (2019). Structural characterization of a galactan from Dioscorea opposita Thunb. and its bioactivity on selected Bacteroides strains from human gut microbiota. *Carbohydrate Polymers, 218*, 299–306. https://doi.org/10.1016/j.carbpol.2019.04.084

Zhang, H., Zhong, J., Zhang, Q., Qing, D., & Yan, C. (2019). Structural elucidation and bioactivities of a novel arabinogalactan from Coreopsis tinctoria. *Carbohydrate Polymers, 219*, 219–228. https://doi.org/10.1016/j.carbpol.2019.05.019